ACCEPTED MANUSCRIPT

SUBMISSION TO GEOMECHANICS FOR ENERGY AND ENVIRONMENT

DATE:

TITLE: Effective stresses for unsaturated states stemming from clay microstructure

AUTHORS:
Matteo Pedrotti*
Alessandro Tarantino **

POSITION AND AFFILIATION:
* Research Fellow, Department of Civil and Environmental Engineering, University of Strathclyde
** Professor, Department of Civil and Environmental Engineering, University of Strathclyde

CONTACT ADDRESS:
Dr. Matteo Pedrotti
Department of Civil and Environmental Engineering
University of Strathclyde
James Weir Building - Level 5
75 Montrose Street - Glasgow G1 1XJ, Scotland, UK
E-mail: matteo.pedrotti@strath.ac.uk

KEYWORDS
Effective stress, microstructure, pore size distribution, unsaturated clay, compacted clay, wetting, shear strength.

ACCEPTED MANUSCRIPT

ACCEPTED MANUSCRIPT

M. Pedrotti & A. Tarantino
'Effective stresses for unsaturated states stemming from clay microstructure'
Submitted to Geomechanics for Energy and Environment

EFFECTIVE STRESSES FOR UNSATURATED STATES STEMMING FROM CLAY MICROSTRUCTURE

M. Pedrotti & A. Tarantino

ABSTRACT

The paper first discusses a novel microstructure conceptual model for compacted clays based on the assumptions that compacted unsaturated clay is made of a water–saturated part (pores filled with water) and an air-saturated part (pores filled with air). The microstructure conceptual model is exploited to interpret a variety of MIP from the literature. The paper then shows the capability of the two effective stresses for unsaturated states stemming from this microstructure conceptual model to model volume change and shear strength behaviour of compacted clays. The model built around these two effective stresses is based on the assumption that the water saturated part behaves like reconstituted clay under saturated conditions and the air-saturated part behaves like clay compressed from dry powder under dry conditions. As a result, mechanical behaviour of compacted clay is modelled by only considering constitutive parameters from reconstituted clay and clay compressed from dry powder.

ACCEPTED MANUSCRIPT

ACCEPTED MANUSCRIPT

1. INTRODUCTION

The effective stress introduced by Terzaghi (1936) for saturated/dry geomaterials was established on an experimental basis 'a*ll measurable effects of a change of stress, such as compression, distortion and a change of shearing resistance are due exclusively to changes in effective stress*'. The liaison of the effective stress with 'measurable' effects makes this concept essentially an experimental result rather than a theory or a principle. Nonetheless, attempts have been made to justify this 'principle' based on simple micro-mechanical models. Bishop (1959) considered an assemblage of inert and sub-rounded particles (granular material) and showed that the effective stress can be interpreted as the '*part of the local contact stress which is in excess of the fluid pressure*'. This micro-mechanical view of the effective stress was further developed and validated experimentally by (Skempton, 1960).

For the case of unsaturated geomaterials, an experimental evidence justifying the use of net stress and matric suction as effective stresses for unsaturated soils was provided by (Fredlund and Morgenstern, 1977)) and Tarantino et al. (2000). Later on, a number of effective stress pairs have been proposed based on either thermodynamics considerations within the continuum mechanics framework (e.g. Houlsby (1997) or micro-scale considerations on the basis of the different states of water in an unsaturated granular material (Buisson and Wheeler, 2000, Gallipoli et al., 2003).

However, none of these effective stress pairs have been validated experimentally (e.g. via null-type tests) or interpreted via micro-mechanical conceptual models similar to the one presented by Bishop (1960). In addition, these effective stresses are based on a micro-scale representation of soils that is essentially associated with granular materials. For example, effective stress pairs proposed by Buisson and Wheeler (2000), Gallipoli et al. (2003), Wheeler et al. (2003) are based on the assumption that water in the pore space is present in the

ACCEPTED MANUSCRIPT

form of either bulk water or meniscus water. This concept is intuitive for granular materials (made of inert and sub-spherical particles) but not for clayey geomaterials. No attempts have been made to reconcile the 'granular' framework commonly used to justify the proposed pairs of effective stresses with the complex microstructure of compacted clays as recognised from Mercury Intrusion Porosimetry (MIP) and Scanning Electron Microscope (SEM) testing.

Pedrotti and Tarantino (2018) have revisited the microstructure of clays encompassing both compacted and reconstituted clays. They formulated a conceptual microstructural model for unsaturated soil, alternative to the traditional 'aggregate-based' microstructural model, based on the assumption that macro-pores are filled with air and micro-pores are filled with water. In turn, this led to two microstructurally-based effective stresses, controlling the response of the air-saturated and water-saturated parts respectively. The practical advantage of these two effective stresses is that the modelling of complex hydro-mechanical paths in compacted unsaturated clays only requires constitutive parameters derived from clay reconstituted from slurry (and tested under saturated state) and clay formed from dry powder (and tested under dry conditions).

This paper further explores the conceptual microstructural model presented by Pedrotti and Tarantino (2018) by showing its capability to interpret a variety of MIP from the literature. It then shows how the two pair of proposed effective stress and the model derived therefrom is capable of modelling volume change behaviour by considering additional hydro-mechanical paths from the literature different from those examined by Pedrotti and Tarantino (2018). In addition, it demonstrates that this pair of effective stresses is also capable of modelling shear strength behaviour of compacted unsaturated clays.

ACCEPTED MANUSCRIPT

2. THE MICROSTRUCTURAL MODEL FOR COMPACTED CLAYS

Microstructure of compacted soils has been extensively studied by means of Mercury Intrusion Porosimetry (MIP) and Scanning Electron Microscope (SEM). Soils compacted on the dry side of optimum and at optimum water content typically show a bi-modal pore size distribution. This is generally taken as an indication of an aggregated structure (Cui and Delage (1996), Romero and Simms (2008), Monroy et al. (2010)). Macro-pores are related to pores between aggregates (inter-aggregate porosity) and micro-pores are related to pores within the aggregates (intra-aggregate porosity) as shown in Figure 1 (Alonso et al. (1987), Delage et al. (1996), Romero et al. (1999), Delage et al. (2006), Alonso et al. (2010), Delage (2010), Monroy et al. (2010), Romero et al. (2011), Casini et al. (2012), Alonso et al. (2012)).

This conceptual microstructural model has gained wider acceptance in the last two decades. The second generation of hydro-mechanical constitutive frameworks for partially saturated clays have been based on the assumption that clay particles form aggregates and the aggregates represent the elementary unit of the clay microstructure rather than individual particles. The literature is rich of contributions on the 'aggregate' nature of compacted unsaturated soils including Delage and Lefebvre (1984), Delage et al. (1996), Romero et al. (1999), Delage et al. (2006), Romero and Simms (2008), Tarantino and De Col (2008), Romero et al. (2011) and Tarantino (2010). This concept has also led to the formulation of successful macroscopic constitutive models, often incorporating microstructural parameters (Gallipoli et al., 2003, Tarantino, 2007, Alonso et al., 2012).

Nonetheless, the 'aggregate' model still presents aspects that are contradictory or controversial if one inspects pore-size distributions at formation (compacted and reconstituted clays). Tarantino and De Col (2008) observed that the characteristic pore size associated with micro- and macro-porosities in compacted kaolin remain the same from very low water

ACCEPTED MANUSCRIPT

contents (dry-side of optimum) up to the water content at optimum.

Pedrotti and Tarantino (2018) carried out an experimental investigation to explore the microstructure of compacted kaolin clay and its interplay with the microstructure of clays reconstituted from slurry and compressed from dry powder. They showed that the PSD of kaolin reconstituted from slurry (formed water-saturated) and kaolin compressed from dry powder (formed air-saturated) overlap astonishingly with the modal sizes associated with the micro- and macro-pores of the compacted samples (Figure 2a).

The straightforward conclusion drawn by Pedrotti and Tarantino (2018) is that, in compacted samples, macro-pores are filled with air and micro-pores are filled with water (Figure 2b). Accordingly, the microstructure of a compacted sample can be assumed to be the 'sum' of the PSDs of the wet (saturated) and dry part as shown in Figure 3. This is an unusual view of micro-structure of unsaturated compacted soils and this concept is explored further in the paper. In particular, it will be shown that the particle-based conceptual model is capable of explaining, at qualitative level, key features of microstructural response of unsaturated compacted clays.

3. PROBING THE PARTICLE-BASED MICROSTRUCTURAL CONCEPTUAL MODEL

3.1. Evolution of pore size distribution at different compaction water contents

Two of the PSDs of compacted kaolin shown in Figure 2a are plotted again in Figure 4a(w=0.22 and w=0.28). The pore space occupied by water is also visualised in Figure 4a (shaded area) and was derived by assuming that the measured pore-water volume saturates the smallest pores. It can be observed clearly that water only occupies the micro-pores, which is

ACCEPTED MANUSCRIPT

consistent with the assumption that micro-pores are the water-saturated pores in the particle-based microstructural conceptual model. It can also be observed that the higher the water content (w=0.28) the higher is the frequency of the micro-pores, which is consistent with the prediction of the particle-based microstructural model. As shown in Figure 4b and Figure 4c, the particle-based model predicts higher frequency of the micro-pores (water saturated) as the water content increases.

It is interesting to notice that similar redistribution of the void ratio frequency as compaction water content is varied has been observed by Casini et al. (2012). In this case, an aeolian silt with 25% non-active clay fraction was compacted at void ratio e=0.5 and water contents of 13%, 15%, 18%, and 18.6% (Figure 5). The PSDs present two dominant sizes (modal values) which remain essentially uncharged throughout the entire range of compaction water contents. As water content increases, the volume associated with the micro-pores increases and the one associated with the macro-pores decreases.

It is also interesting to note that Figure 2a and Figure 5 shows an inconsistency of the 'aggregated-based' microstructural model (i.e. macro-pores associated with inter-aggregate porosity and micro-pores associated with intra-aggregate porosity). As compaction water content decreases, the volume of voids associated with intra-aggregate pores is observed to decrease experimentally and, hence, aggregates disappear. However, the volume of voids associated with inter-aggregate pores increases, which leads to the paradox that additional inter-aggregate pores form while the number of aggregates reduces! This undermines the association generally made between macro-pores and inter-aggregate pores and, hence, that double-porosity implies aggregate microstructure.

ACCEPTED MANUSCRIPT

3.2. Evolution of the pore size distribution upon wetting

Monroy (2006) presented the evolution of the pore size distribution of compacted samples of London clay (58% clay) upon wetting under free-swelling conditions. Samples were compacted to a dry density of 1.384 (Mg/m^3) and degree of saturation of about 67%. Samples were then subjected to a wetting and were then dehydrated by means of freeze-drying technique and tested in the MIP. The evolution of the pore size upon wetting is reported in Figure 6.

Experimental data show micro-pores increase in size and volume whilst the macro-pores tend to disappear (macro-pore size remains unchanged steady while the associated volume reduces). According to the particle-based conceptual framework, two types of mechanisms are expected to occur upon saturation (Figure 7):

i) Water-saturated pores rebound due to the decrease in suction
ii) Air-saturated pores become water-saturated and collapse (inter-particle distance adjusts to the new pore fluid).

As a result, one would expect water-saturated part to increase its volume and the initially air-saturated part to reduce its volume (collapse). The overall volume can therefore either increase or decrease depending on the dominating mechanism. The evolution of the PSD predicted by the 'particle-based' model is shown in Figure 8. An initial decrease in suction causes an increase in the micro-pore size as well as the micro-pore volume. The macro-pores do not change in modal size (which still remains the one associated with the air-saturated particles) but their volume decreases (due to the inter-particle space that becomes water-saturated). Eventually, only water-saturated pores are present and the PSD shows it to be mono-modal. This pattern matches the experimental observation in Figure 6.

ACCEPTED MANUSCRIPT

3.3. Evolution of the pore size distribution: drying

Figure 9 shows the void ratio versus suction of kaolin clay consolidated from slurry to 100 kPa and then air-dried (after Tarantino (2010). The clay remains saturated below the air-entry suction and therefore moves along the normal consolidation line. Beyond the air-entry suction, the void ratio shows a tendency to become constant before increasing at high suction. This macroscopic behaviour can be explained qualitatively by the particle-based microstructural model.

When an initially saturated sample is subjected to an increase in suction (drying path) then :

i) Water-saturated pores reduce in size as suction increases until the meniscus does not recede into the pores
ii) Pores that desaturate are expected to rebound because of the release of suction when the inter-particle space is replaced by air (Figure 10).

The overall volume change behaviour beyond the air-entry suction is the sum of these two competing mechanisms. The apparent steady-state achieved beyond the air-entry would be the result of a balance between these two mechanisms. At high suctions, the rebound of the pores that desaturate would be expected to dominate therefore returning an overall increase in void ratio.

4. MODELLING VOLUME CHANGE BEHAVIOUR

4.1. Microstructure-based effective stresses for the mechanical behaviour of unsaturated soils

The conceptual model discussed in the previous sections led to the assumption of two separate effective stresses (Pedrotti and Tarantino 2018), one acting on the water-saturated fraction of the sample, σ'_W (equation [1]), and the other acting on the air-saturated fraction, σ'_A (equation [2]):

ACCEPTED MANUSCRIPT

$$\sigma'_W = (\sigma - u) \cdot S_r \quad [1]$$

$$\sigma'_A = (\sigma - u) \cdot (1 - S_r\ ) \quad [2]$$

Based on this definition of effective stresses, Pedrotti and Tarantino (2018) formulated a microstructurally-based constitutive model for the volumetric behaviour based on four main hypotheses, which are summarised hereafter for sake of convenience:

1. 4 classes of pores are considered.
   - Pores that are water-saturated before and after the change in effective stress σ'_W. Such pores are indicated with the subscript –WW.
   - Pores that are air-saturated before and after the change in effective stress σ'_A. Such pores are indicated with the subscript –AA.
   - Pores that experienced a fluid transition that are initially air-saturated and become water-saturated upon a positive change in degree of saturation, ΔS_r. Such pores are indicated with the subscript –AW.
   - Pores that experienced a fluid transition that are initially water-saturated and become air-saturated upon a negative change in degree of saturation, ΔS_r. Such pores are indicated with the subscript –WA.
2. Water-saturated pores (-WW and –AW) have the same set of compressibility curves (either normal consolidation lines, ncl, or unloading and reloading lines, url) and air-saturated pores (-AA and –WA) have another set of compressibility curves (either ncl or url) regardless of their origin.
3. Water-saturated pores mechanical response is the one of clay reconstituted from slurry and air-saturated pores mechanical response is the one of dry powder.
4. Saturated pores are combined as a function of ΔS_r and air-saturated pores as a function of (1- ΔS_r).

Figure 11 shows the flow chart representing the approach to the modelling. The model is not discussed here, but two case studies are presented in order to provide an insight of the model.

$\Delta\sigma$, Δu and ΔS_R is the change in total stress, pore pressure and degree of saturation respectively. λ_w and κ_w are the slopes of the *ncl* and the *url* for the clay reconstituted from slurry respectively and λ_A and κ_A are the slopes of the *ncl* and the *url* for the clay prepared

ACCEPTED MANUSCRIPT

from dry powder respectively. Δe^{WW}, Δe^{AW}, Δe^{AA}, Δe^{WA} is the change in void ratio associated to the four classes of pores, e^W and e^A the void ratio associated to the water saturated pores and to the air-saturated pores respectively, and *e* the void ratio of whole sample. The functions for the combination of the water saturated pores and for the combination of the air-saturated pores (derived in Pedrotti and Tarantino (2018)) are reported in equation [3] and [4]:

$$\Delta e^W = \Delta e^{WW} \cdot \left[1 - \frac{\Delta S_r}{S_r}\right] + \Delta e^{AW} \frac{\Delta S_r}{S_r} \quad [3]$$

$$\Delta e^A = \Delta e^{AA} \cdot \left[1 - \frac{(-\Delta S_r)}{1 - S_r}\right] + \Delta e^{WA} \frac{(-\Delta S_r)}{1 - S_r} \quad [4]$$

The coupling equation, already derived in Pedrotti and Tarantino (2018) is:

$$\mathrm{e} = \frac{e^W + e^A}{e^W(1 - S_R) + e^A S_R} \quad [5]$$

A representation of the methodology employed for the modelling is sketched in Figure 12a.

4.2. Case study

Tests presented by Sivakumar and Wheeler (2000) are considered as case study. Speswhite kaolin was compacted at constant water content (25%) to 400 and 800 kPa vertical stress respectively (point A in Figure 13) and then unloaded to 15 kPa (point B in Figure 13). Suction was then decreased to either 100 or 300 kPa at constant mean net stress (wetting path, point C in Figure 13). After wetting, the samples were re-loaded isotropically up to 200 kPa (point D in Figure 13) at constant suction (either 100 or 300 kPa).

Modelling unloading at constant water content

As reported in section 5.1, the hypothesis 3 states that the mechanical response of the pores is

ACCEPTED MANUSCRIPT

governed by the ncl (or url) of clay reconstituted from slurry and by the ones of dry powder.

In order to ease the readability of the figures reporting the volumetric paths in terms of void ratio and effective stress, the ncl line of a sample reconstituted from slurry and the ncl of a sample prepared as dry powder are reported in every figure and used as reference.

At the end of compaction (point A in Figure 13) only two different classes of pores are present: i) water-saturated pores and ii) air-saturated pores (Figure 14).

At this stage, the void ratio of the compacted sample is computed according to equation [5] as the combination between the void ratio of the air-saturated pores and the void ratio of the water-saturated ones, weighted by a the degree of saturation.

As the total stress is decreased, the degree of saturation decreases, i.e. the samples are subjected to a mechanically induced drying.

Upon unloading, three different paths have to be considered for the pores and therefore three different classes of pores. Air-saturated pores remain air-saturated and therefore move along the air-saturated unloading-reloading line (*url*). The change in void ratio $(\Delta e^{AA})_{url}$ can be calculated according to the constitutive law reported in equation [2] (Figure 14):

$$(\Delta e^{AA})_{url} = -k_A \, \Delta(ln\sigma'_A) \qquad [6]$$

On the other hand, a part of the water-saturated pores remains water-saturated and a part of the initially water-saturated pores becomes air-saturated (fluid transition). The former moves along the water-saturated *url* and are subject to a change in void ratio $(\Delta e^{WW})_{url}$ (Figure 14). The constitutive equation is reported in equation [7]:

$$(\Delta e^{WW})_{url} = -k_W \, \Delta(ln\sigma'_W) \qquad [7]$$

The water-saturated pores that become air-saturated, moves from the water-saturated *ncl* to the air-saturated *url* (path Δe^{WA} in Figure 14). For the change of void ratio of the classes of

ACCEPTED MANUSCRIPT

pores subjected to fluid transition (i.e. from water-saturated to air-saturated), it is convenient to introduce an equivalent air-saturated pre-consolidation stress, σ'^{*}_{A} (shown in Figure 14). As shown in Figure 14, this is given by the air-saturated effective stress that returns a void ratio on the air-saturated *ncl* equal to the void ratio before the change of state. Accordingly, the constitutive law for the change in void ratio Δe^{WA} is:

$$(\Delta e^{WA}) = -k_A \ln\left(\frac{\sigma'_A}{\sigma'^{*}_A}\right) \quad [8]$$

These pores also experience volumetric rebound. It is worth noting that upon unloading the change in degree of saturation is small and so the consequent volume change. For the sake of simplicity, this class of pores (resulting from Δe^{WA}) are not discussed taken into consideration in the next sections. However, they were considered during the simulation.

Modelling of wetting at constant total stress

After unloading, samples were wetted at constant stress to a target suction. At the end of the unloading path, three classes of pores are detected. Each class of pores follows its own hydro-mechanical path as shown in Figure 15.

Part of the air-saturated pores remains air-saturated. Because of the increase of ΔS_r, the air-saturated effective stress reduces, and therefore this class experience a rebound as defined by equation [6] (Figure 15).

The rest of the air-saturated pores becomes water-saturated (fluid transition). Such pores experience volumetric collapse as they move to the water-saturated *ncl* (Δe^{AW} in Figure 15). Similarly to what discussed for the Δe^{WA}, it is convenient to introduce an equivalent water-saturated pre-consolidation stress, σ'^{*}_{W}. Therefore, the constitutive law for the change in void ratio Δe^{AW} is:

ACCEPTED MANUSCRIPT

$$(\Delta e^{AW}) = -\lambda_w \ln\left(\frac{\sigma'_W}{\sigma'^*_W}\right) \quad [9]$$

On the other hand, upon wetting, the water-saturated pores that were and remain saturated experience swelling due to the decrease in suction, $(\Delta e^{W})_{url}$ in Figure 15 and equation [7] .

Modelling of compression at constant suction

Upon compression at constant suction, the degree of saturation increases. The air-saturated pores that remain air-saturated move on the air-saturated *url*, $(\Delta e^{A})_{url}$ in Figure 16 and equation [6]. Part of the air-saturated pores becomes water saturated and therefore experience collapse (Δe^{AW} in Figure 16 and equation [9]).

On the other hand, at the beginning of the recompression, two classes of water-saturated pores exist. One class lies on the water-saturated *ncl* and will deform according to the constitutive law reported in equation [10], and the other class of water-saturated pores lies on the water-saturated *url* and will deform according to equation [7].

$$(\Delta e^{WW})_{ncl} = -\lambda_w \, \Delta(ln\sigma'_w) \quad [10]$$

Simulation of hydro-mechanical path

To simulate the hydro-mechanical path reported in Figure 13:

i) The total stress and degree of saturation values under compaction load and after unloading, points A and B respectively in Figure 13, were taken from Sivakumar and Wheeler (2000).

ii) The suction values under compaction load and after unloading, points A and B respectively in Figure 13, were inferred from Tarantino and De Col (2008). For the constant suction path, suction was assumed as reported in Sivakumar and Wheeler (2000)

ACCEPTED MANUSCRIPT

iii) The compressibility indexes (ncl and url) of kaolin reconstituted from slurry and kaolin prepared from dry powder were taken as the only 'constitutive' parameters. These were derived from compression test in oedometer cell reported in Pedrotti and Tarantino (2018) and Pedrotti (2016). The specific volume a 1 kPa for both water-saturated and air-saturated samples, was calculated by assuming a k_0 value of 0.77. Such value was back calculated in order to match the void ratio in A (Figure 13)

The simulation is compared with the experimental data from Sivakumar and Wheeler (2000) in Figure 17. The simulation captures the experimental data fairly well considering that the only constitutive parameters considered in the simulation are associated with the behaviour of clay formed water-saturated (reconstituted) and compressed under saturated conditions and clay formed air-saturated (compressed from dry powder) and compressed under dry conditions.

5. MODELLING SHEAR STRENGTH BEHAVIOUR

5.1. Average skeleton shear strength

The shear strength is assumed to be a weighted average of the shear strength mobilised in the water-saturated and air-saturated part of the clay. To this end, let us consider the equilibrium of the shear forces across a shear plane of area *A*:

$$T = \tau A = T^w + T^A \quad [11]$$

where T is the shear force acting on the shear plane, T^W and T^A are the components of T acting respectively on the wet and dry part, and τ is average shear stress. The shear stress associated to the wet part, τ^W and the one associate to the dry part, τ^A, can be defined as

ACCEPTED MANUSCRIPT

follows:

$$wet:\ T^W = \tau^W A^W \ \rightarrow\ \tau^W = \frac{T^W}{A^W} \qquad [12]$$

$$dry:\ T^A = \tau^A A^A \ \rightarrow\ \tau^A = \frac{T^A}{A^A}$$

Therefore the total shear stress τ^c can be written as:

$$\tau \ = \frac{T^w}{A} + \frac{T^A}{A} = \frac{T^w}{A^W} \cdot \frac{A^W}{A} + \frac{T^A}{A^A} \cdot \frac{A^A}{A} = \tau^W \cdot \frac{A^W}{A} + \tau^A \cdot \frac{A^A}{A} \qquad [13]$$

By assuming that the term $\frac{A^W}{A}$ equals the degree of saturation S_R, we can therefore write:

$$\tau \ = \tau^W \cdot S_R + \tau^A \cdot (1 - S_R) \qquad [14]$$

Equation 19 shows that the tangential stress τ can be expressed as an average of the tangential stresses τ^W and τ^A acting on the wet and dry part respectively weighted by the degree of saturation, S_R. The assumption made in this work is that τ^W is controlled by the effective stress controlling the wet part, $\sigma'_w = (\sigma - u_w)S_R$, and that τ^A is controlled by the effective stress controlling the dry part $\sigma'_A = (\sigma - u_A)(1 - S_R)$.

5.2. Simulation of shear strength

Ultimate shearing resistance of kaolin clay compacted at different water contents and vertical stress was investigated in order to validate the model. Direct shear experimental data were taken from Tarantino and Tombolato (2005). Thirty-three samples compacted to 300, 600 and 900 kPa vertical stress and having water content ranging from w= 0.24 to w=0.34 were sheared. Shearing was made in a modified direct shear cell where suction was measured by high-capacity tensiometers.

To derive the reference states for (reconstituted) water-saturated and air-saturated (dry)

ACCEPTED MANUSCRIPT

clay, kaolin reconstituted from slurry was consolidated in a direct shear box to 100, 300, 450, 700 and 1200 kPa vertical stress and then sheared. According to Tarantino and Tombolato (2005) the same horizontal displacement rate of 8mm/day was adopted for the set of saturated samples. The shear strength envelope for the reconstituted water-saturated kaolin is shown in Figure 18.

Furthermore, oven dried powder was compressed to 50, 100, 150, 300, 600, 900 and 1200 kPa vertical stress in the direct shear box. After compression, the samples were sheared at horizontal displacement rate of 0.5mm/day. The shear strength envelope for the air-saturated kaolin (dry powder) is shown in Figure 18.

Figure 19 shows the experimental data for the ultimate shear strength of the partially saturated samples together with the simulation in the plane ultimate shear stress, τ, versus applied vertical stress, σ. The quality of the prediction is shown in Figure 20 and it appears to be comparable with the accuracy of the prediction according to the approach proposed by Tarantino and Tombolato (2005). Again, it is remarkable that the only constitutive parameters considered in the simulation are associated with the behaviour of clay formed water-saturated (reconstituted) and sheared under saturated conditions and clay formed air-saturated (compressed from dry powder) and sheared under dry conditions (as sketched in Figure 12b).

6. CONCLUSIONS

The paper discussed an alternative microstructural conceptual model for compacted clays. based on the assumption that that the two modal pore-size in the PSD are associated with pores that are either filled with water (water-saturated) or filled with air (air-saturated). This microstructural conceptual model has proven to interpret correctly the pore-size distribution of samples as-compacted and samples subjected to wetting and drying path. In particular, the

ACCEPTED MANUSCRIPT

microstructural conceptual model appears to explain the pore-size distribution pattern observed in samples compacted at very low water content in contrast with the aggregate model.

Stemming from this microstructural view of compacted clays, two effective stresses were assumed to control the behaviour of the air-saturated and water-saturated parts respectively. In addition, it was assumed that the water-saturated part of the compacted clay behaves as the clay reconstituted from slurry and the air-saturated part behaves as the clay compressed from dry powder. Accordingly, constitutive parameters for volume change and shear strength behaviour could be derived from tests on reconstituted and dry clay. It has been then shown that this approach can successfully simulate relatively complex hydro-mechanical volume change and shear strength behaviour of compacted clay.

NOTATION LIST

σ'_W - effective stress acting on the water-saturated fraction [kPa]

σ'_A - effective stress acting on the air-saturated fraction [kPa]

σ'^*_W - equivalent water-saturated pre-consolidation stress [kPa]

σ – mean net stress [kPa]

$\Delta\sigma$ – change in total stress [kPa]

u – pore water pressure [kPa]

Δu – change in pore water pressure [kPa]

S_r - Degree of saturation [-]

ΔS_r - Change in degree of saturation [-]

w – water content [-]

e – void ratio [-]

ACCEPTED MANUSCRIPT

e^W – void ratio associated to the water-saturated pores

e^A - void ratio associated to the air-saturated pores

Δe^W – change in void ratio associated to the water-saturated pores

Δe^A – change in void ratio associated to the air-saturated pores

Δe^{WW} – change in void ratio of pores that are water-saturated before and after the change in effective stress σ'_W

Δe^{AA} – change in void ratio of pores that are air-saturated before and after the change in effective stress σ'_A

Δe^{AW} – change in void ratio of pores that experienced a fluid transition that are initially air-saturated and become water-saturated upon a positive change in degree of saturation, ΔS_r

Δe^{WA} – change in pores that experienced a fluid transition that are initially water-saturated and become air-saturated upon a negative change in degree of saturation, ΔS_r

λ_w – slope of the normal consolidation line (ncl) for clay reconstituted from slurry

κ_w - slope of the unloading reloading line (url) for clay reconstituted from slurry

λ_A – slope of the normal consolidation line (ncl) for clay prepared from dry powder

κ_A - slope of the unloading reloading line (url) for clay prepared from dry powder

T – shear force acting on the shear plane [kN]

T^W - component of the shear force acting on the water-saturated fraction [kN]

T^A - component of the shear force acting on the air-saturated fraction [kN]

τ - average shear stress [kPa]

τ^W - shear stress associated to the water-saturated fraction [kPa]

τ^A - shear stress associated to the air-saturated fraction [kPa]

A – area of the shear plan [m^2]

ACCEPTED MANUSCRIPT

A^W – water-saturated fraction of the area of the shear plan [m^2]

A^A – air-saturated fraction of the area of the shear plan [m^2]

ACCEPTED MANUSCRIPT

ACCEPTED MANUSCRIPT

7. REFERENCES

ALONSO, E., GENS, A. & HIGHT, D. Special problem soils. General report. Proceedings of the 9th European conference on soil mechanics and foundation engineering, Dublin, 1987. 1087-1146.

ALONSO, E., PINYOL, N. & GENS, A. 2012. Compacted soil behaviour: initial state, structure and constitutive modelling. *Geotechnique,* 63**,** 463-478.

ALONSO, E. E., PEREIRA, J.-M., VAUNAT, J. & OLIVELLA, S. 2010. A microstructurally based effective stress for unsaturated soils. *Geotechnique,* 60**,** 913-925.

BISHOP, A. W. 1960. *The principles of effective stress*, Norges Geotekniske Institutt.

BUISSON, M. & WHEELER, S. 2000. Inclusion of hydraulic hysteresis in a new elastoplastic framework for unsaturated soils. *Experimental evidence and theoretical approaches in unsaturated soils***,** 109-119.

CASINI, F., VAUNAT, J., ROMERO, E. & DESIDERI, A. 2012. Consequences on water retention properties of double-porosity features in a compacted silt. *Acta Geotechnica,* 7**,** 139-150.

CUI, Y. & DELAGE, P. 1996. Yielding and plastic behaviour of an unsaturated compacted silt. *Geotechnique,* 46**,** 291-311.

DELAGE, P. 2010. A microstructure approach to the sensitivity and compressibility of some Eastern Canada sensitive clays. *Geotechnique,* 60**,** 353-368.

DELAGE, P., AUDIGUIER, M., CUI, Y.-J. & HOWAT, M. D. 1996. Microstructure of a compacted silt. *Canadian Geotechnical Journal,* 33**,** 150-158.

DELAGE, P. & LEFEBVRE, G. 1984. Study of the structure of a sensitive Champlain clay and of its evolution during consolidation. *Canadian Geotechnical Journal,* 21**,** 21-35.

DELAGE, P., MARCIAL, D., CUI, Y. & RUIZ, X. 2006. Ageing effects in a compacted bentonite: a microstructure approach. *Geotechnique,* 56**,** 291-304.

FREDLUND, D. G. & MORGENSTERN, N. R. 1977. Stress state variables for unsaturated soils. *Journal of Geotechnical and Geoenvironmental Engineering,* 103.

GALLIPOLI, D., GENS, A., SHARMA, R. & VAUNAT, J. 2003. An elasto-plastic model for unsaturated soil incorporating the effects of suction and degree of saturation on mechanical behaviour. *Géotechnique.,* 53**,** 123-136.

HOULSBY, G. 1997. The work input to an unsaturated granular material. *Géotechnique,* 47**,** 193-196.

MONROY, R. 2006. *The influence of load and suction changes on the volumetric behaviour of compacted London Clay.* Imperial College London (University of London).

MONROY, R., ZDRAVKOVIC, L. & RIDLEY, A. 2010. Evolution of microstructure in compacted London Clay during wetting and loading. *Geotechnique,* 60**,** 105-119.

PEDROTTI, M. 2016. *An experimental investigation on the micromechanics of non-active clays in saturated and partially-saturated states.* Ph.D. Thesis, University of Strathclyde, Glasgow, Scotland, UK.

PEDROTTI, M. & TARANTINO, A. 2018. A conceptual constitutive model unifying slurried (saturated), compacted (unsaturated) and dry states. *Geotechnique - provisionally accepted*.

ROMERO, E., DELLA VECCHIA, G. & JOMMI, C. 2011. An insight into the water retention properties of compacted clayey soils. *Geotechnique,* 61**,** 313.

ACCEPTED MANUSCRIPT

ROMERO, E., GENS, A. & LLORET, A. 1999. Water permeability, water retention and microstructure of unsaturated compacted Boom clay. *Engineering Geology,* 54**,** 117-127.

ROMERO, E. & SIMMS, P. H. 2008. Microstructure investigation in unsaturated soils: a review with special attention to contribution of mercury intrusion porosimetry and environmental scanning electron microscopy. *Geotechnical and Geological Engineering,* 26**,** 705-727.

SIVAKUMAR, V. & WHEELER, S. 2000. Influence of compaction procedure on the mechanical behaviour of an unsaturated compacted clay. Part 1: Wetting and isotropic compression. *Géotechnique,* 50**,** 359-368.

SKEMPTON, A. 1960. Terzaghi's discovery of effective stress. *From Theory to Practice in Soil Mechanics: Selections from the Writings of Karl Terzaghi***,** 42-53.

TARANTINO, A. 2007. A possible critical state framework for unsaturated compacted soils. *Geotechnique,* 57**,** 385-389.

TARANTINO, A. Unsaturated soils: compacted versus reconstituted states. 5th International Conference on Unsaturated Soil, 2010. 113-136.

TARANTINO, A. & DE COL, E. 2008. Compaction behaviour of clay. *Geotechnique,* 58**,** 199-213.

TARANTINO, A., MONGIOVI, L. & BOSCO, G. 2000. An experimental investigation on the independent isotropic stress variables for unsaturated soils. *Geotechnique,* 50**,** 275-282.

TARANTINO, A. & TOMBOLATO, S. 2005. Coupling of hydraulic and mechanical behaviour in unsaturated compacted clay. *Geotechnique,* 55**,** 307-317.

TERZAGHI, V. K. The shearing resistance of saturated soils and the angle between the planes of shear. Proceedings of the 1st international conference on soil mechanics and foundation engineering, 1936. 54-56.

WHEELER, S., SHARMA, R. & BUISSON, M. 2003. Coupling of hydraulic hysteresis and stress–strain behaviour in unsaturated soils. *Geotechnique,* 53**,** 41-54.

ACCEPTED MANUSCRIPT

8. LIST OF CAPTIONS FOR ILLUSTRATIONS

Figure 1. 'Aggregate' microstructural model for compacted soils

Figure 2. a) Pore size distribution of compacted kaolin samples (after Tarantino & De Col, 2008) and comparison with PSD of reconstituted kaolin and kaolin compressed from dry powder (after Pedrotti and Tarantino (2018))

Figure 3. Schematic representation of the microstructure and PSD of (a) samples reconstituted from slurry and compressed from dry powder and (b) compacted samples.

Figure 4. **Error! Reference source not found.**

Figure 4. Anticipated pore size distribution for samples compacted at different water content. a) Evolution of pore size distribution of compacted kaolin at different water content and 1200 kPa of vertical stress and comparison with water void ratio (data from Tarantino and De Col (2008)). (b) lower water content; (c) higher water content.

Figure 5. Pore size distribution of aeolian silt compacted at the same void ratio (Casini et al., 2012).

Figure 6. Evolution of pore size distribution of compacted London clay upon wetting (after Monroy (2006)

Figure 7. Conceptual model for inter-particle space evolution upon wetting of compacted kaolin. (a) Micro-pore rebound. (b) Macro-pore collapse

Figure 8. Swelling of two samples compacted at the same water content and different vertical stresses and then saturated.

Figure 9. Volume deformation of reconstituted kaolin from slurry upon drying

Figure 10. Drying mechanism

Figure 12. Propose methodology for constitutive modelling

ACCEPTED MANUSCRIPT

Figure 13. Hydro-mechanical path

Figure 14. Pores macroscopic behaviour of compacted sample upon unloading at constant water content.

Figure 15. Pores macroscopic behaviour upon wetting at constant stress

Figure 16. Pores macroscopic behaviour upon compression at constant suction

Figure 17. Simulation of unloading at constant water content, wetting at constant vertical stress and loading at constant suction. a) Sample compacted to 400 kPa total stress, constant suction path at 100 kPa, b) Sample compacted to 800 kPa total stress, constant suction path at 100 kPa, c) Sample compacted to 400 kPa total stress, constant suction path at 300 kPa and d) Sample compacted to 800 kPa total stress, constant suction path at 300 kPa,

Figure 18. Water-saturated and air-saturated shear envelopes.

Figure 19. Ultimate shear simulation of kaolin compacted at different water contents and vertical stress.

Figure 20 Prediction of the ultimate shear stress against the measured one.

ACCEPTED MANUSCRIPT

ACCEPTED MANUSCRIPT

M. Pedrotti & A. Tarantino
'Effective stresses for unsaturated states stemming from clay microstructure'
Submitted to Geomechanics for Energy and Environment

ILLUSTRATIONS

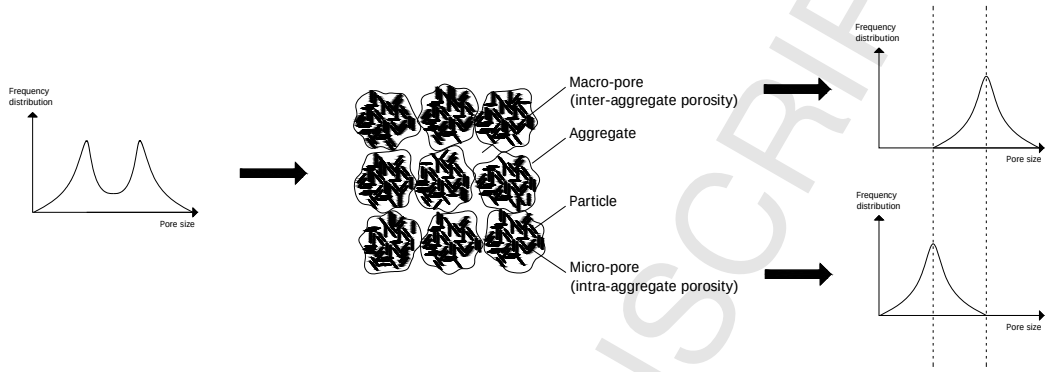

Figure 1. 'Aggregate' microstructural model for compacted soils

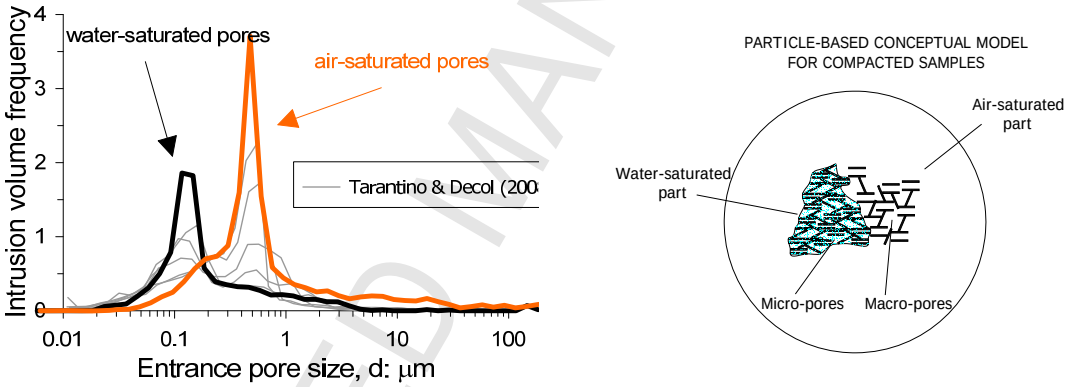

(a) (b)

Figure 2. a) Pore size distribution of compacted kaolin samples (after Tarantino & De Col, 2008) and comparison with PSD of reconstituted kaolin and kaolin compressed from dry powder (after Pedrotti and Tarantino (2018)), b) particle-based conceptual model for compacted samples.

ACCEPTED MANUSCRIPT

ACCEPTED MANUSCRIPT

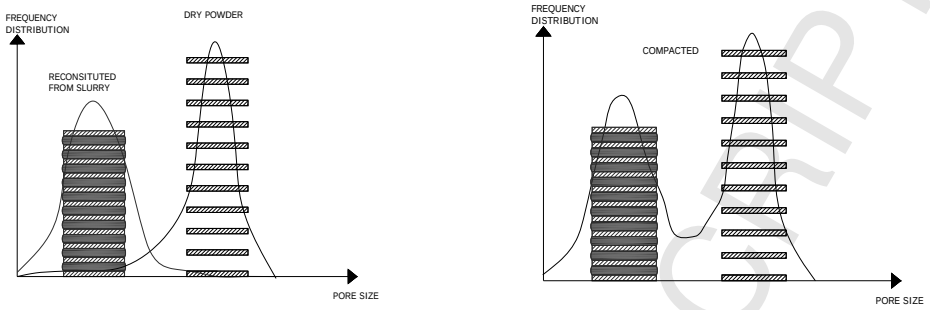

a) b)

Figure 3. Schematic representation of the microstructure and PSD of (a) samples reconstituted from slurry and compressed from dry powder and (b) compacted samples.

ACCEPTED MANUSCRIPT

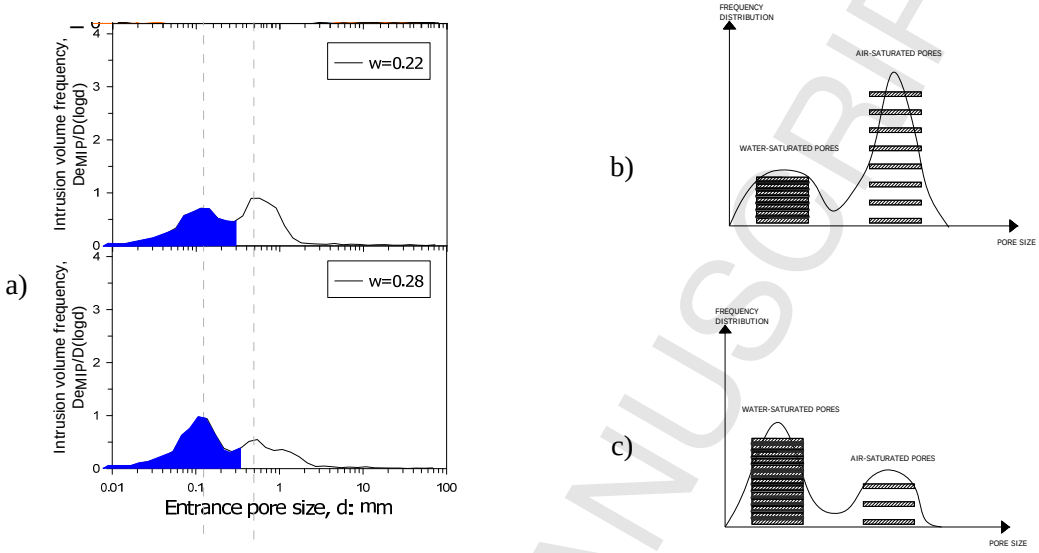

Figure 4. Anticipated pore size distribution for samples compacted at different water content. a) Evolution of pore size distribution of compacted kaolin at different water content and 1200 kPa of vertical stress and comparison with water void ratio (data from Tarantino and De Col (2008)). (b) lower water content; (c) higher water content.

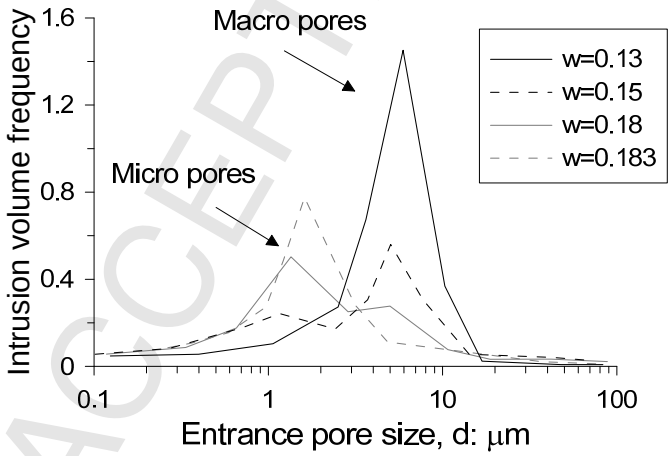

Figure 5. Pore size distribution of aeolian silt compacted at the same void ratio (Casini et al.,

2012).

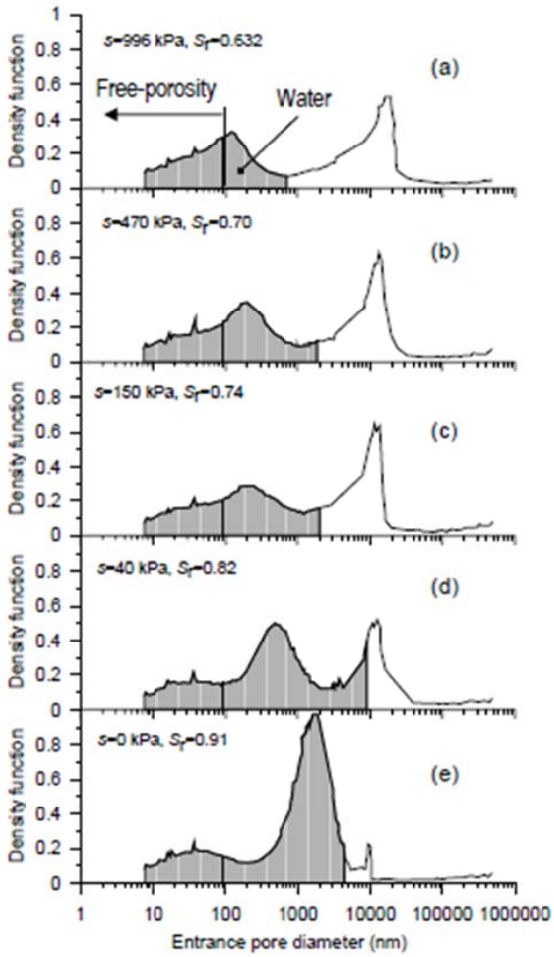

Figure 6. Evolution of pore size distribution of compacted London clay upon wetting (after Monroy (2006)

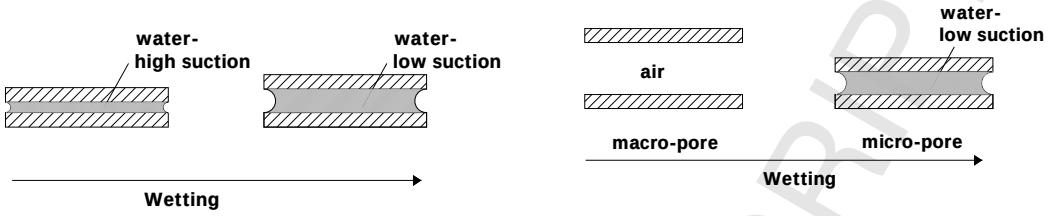

(a) (b)

Figure 7. Conceptual model for inter-particle space evolution upon wetting of compacted kaolin. (a) Micro-pore rebound. (b) Macro-pore collapse

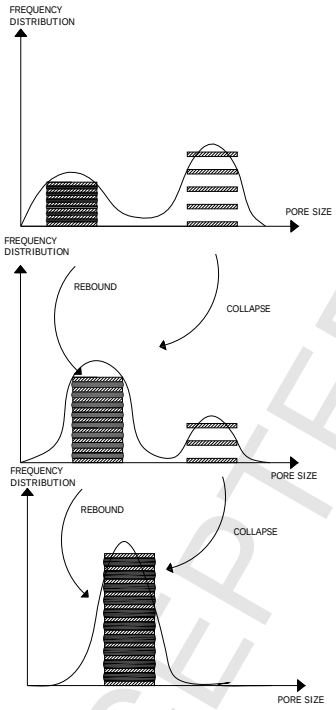

Figure 8. Swelling of two samples compacted at the same water content and different vertical stresses and then saturated.

ACCEPTED MANUSCRIPT

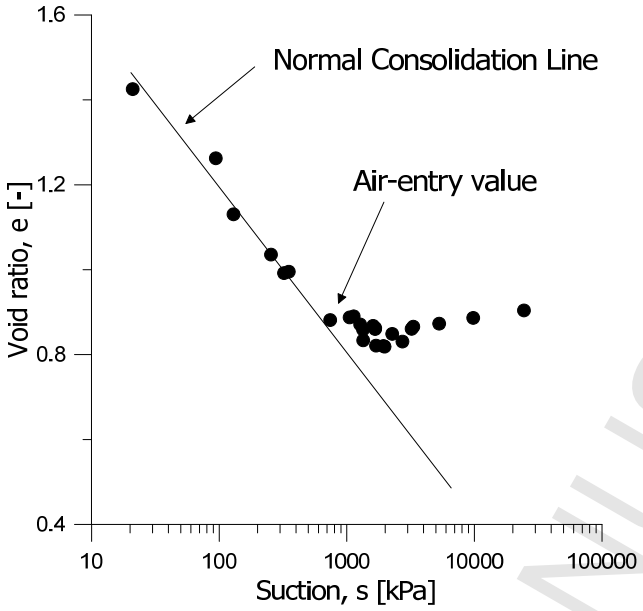

Figure 9. Volume deformation of reconstituted kaolin from slurry upon drying

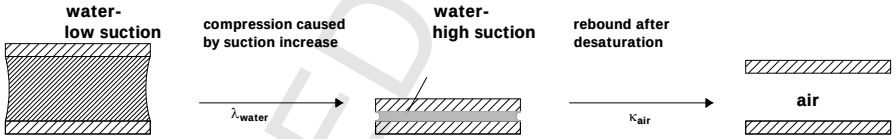

Figure 10. Drying mechanism

ACCEPTED MANUSCRIPT

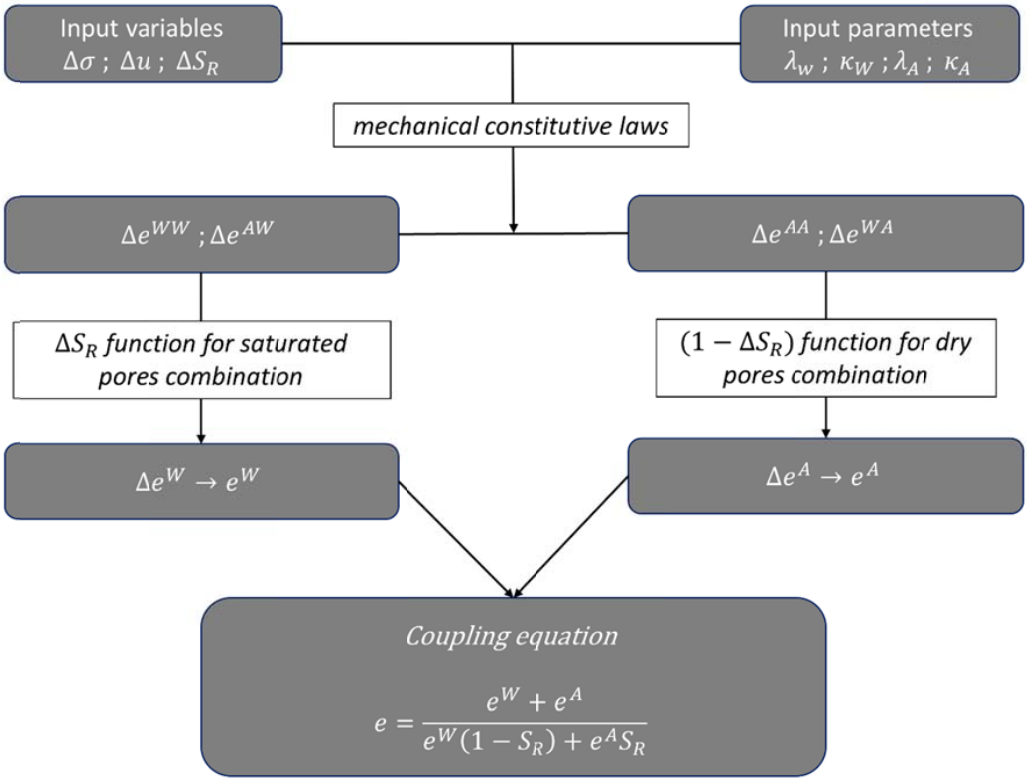

Figure 11. Flow chart on the approach to modelling

ACCEPTED

ACCEPTED MANUSCRIPT

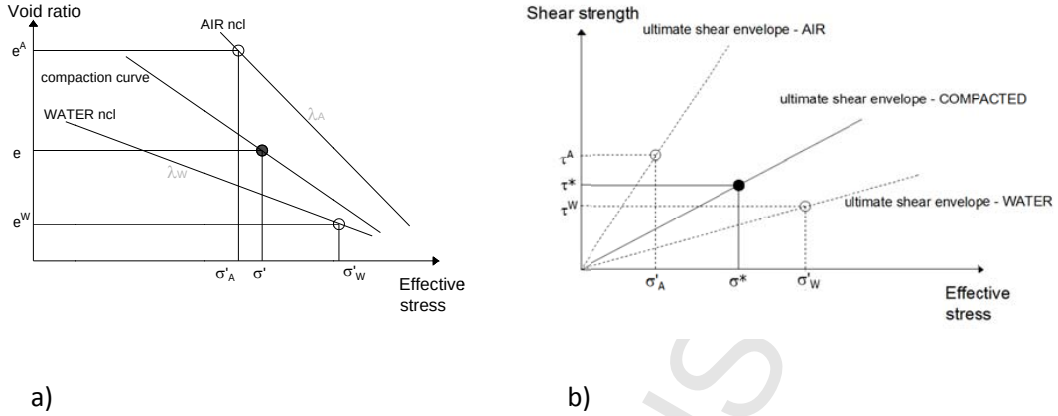

Figure 12. Propose methodology for constitutive modelling

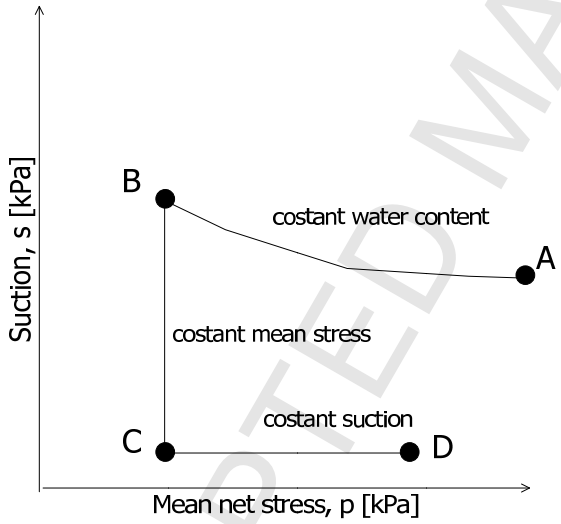

Figure 13. Hydro-mechanical path

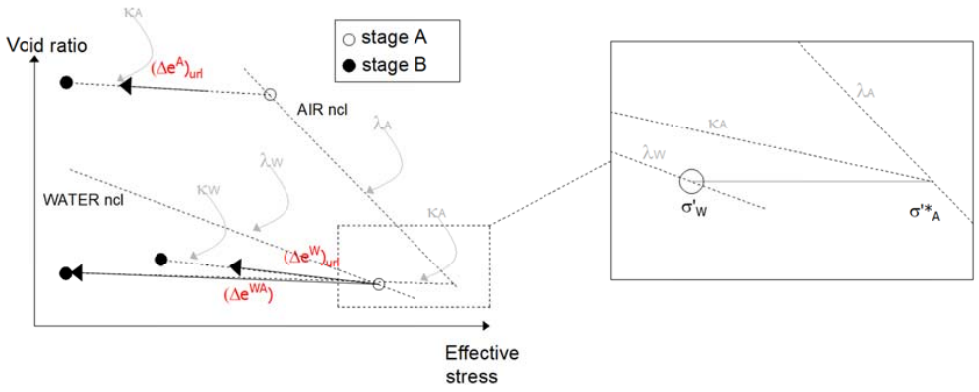

Figure 14. Pores macroscopic behaviour of compacted sample upon unloading at constant water content.

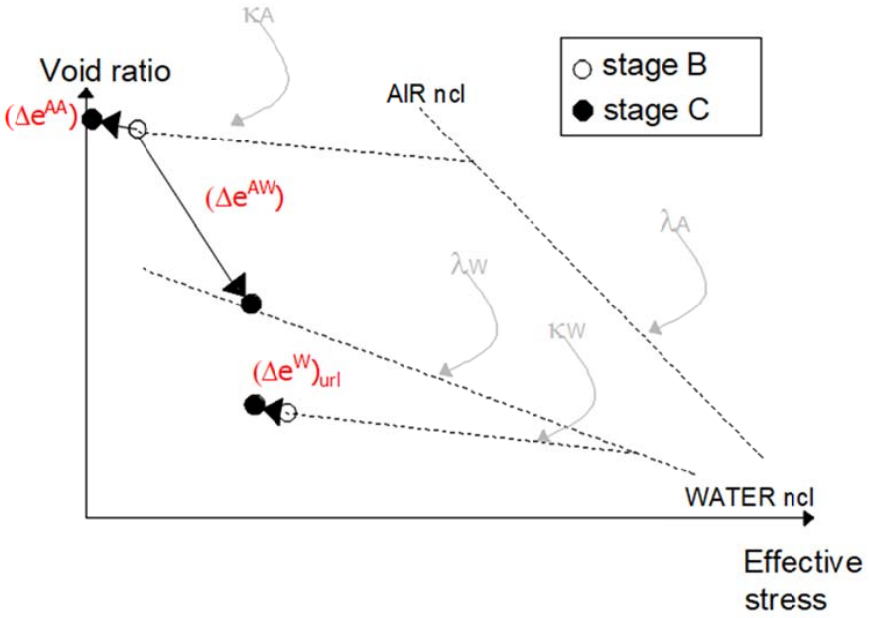

Figure 15. Pores macroscopic behaviour upon wetting at constant stress

ACCEPTED MANUSCRIPT

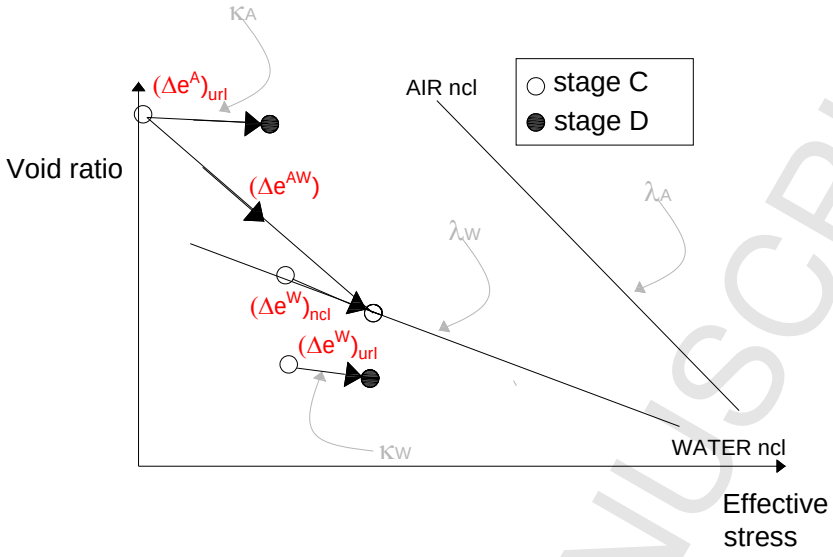

Figure 16. Pores macroscopic behaviour upon compression at constant suction

ACCEPTED MANUSCRIPT

ACCEPTED MANUSCRIPT

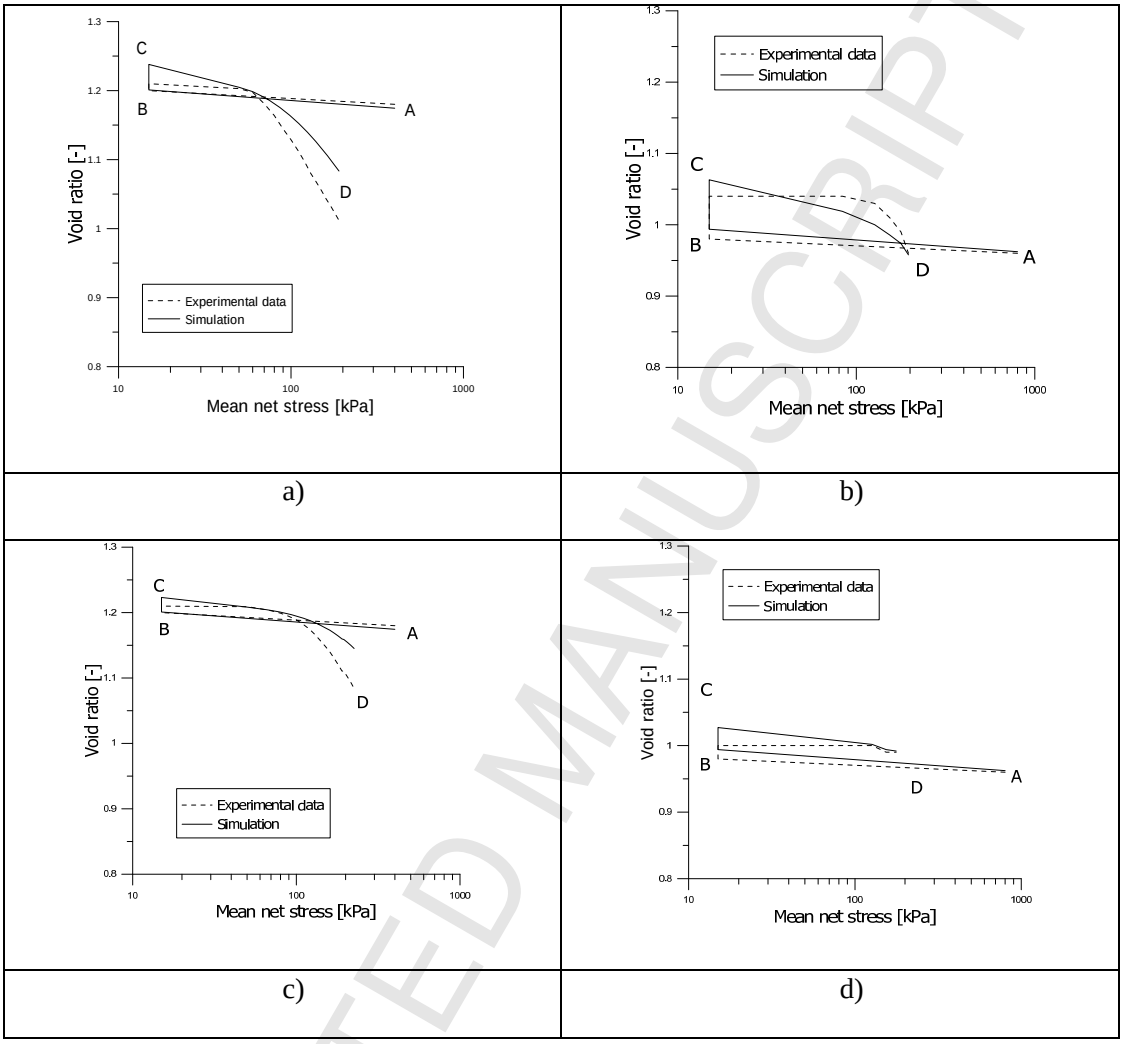

Figure 17. Simulation of unloading at constant water content, wetting at constant vertical stress and loading at constant suction. a) Sample compacted to 400 kPa total stress, constant suction path at 100 kPa, b) Sample compacted to 800 kPa total stress, constant suction path at 100 kPa, c) Sample compacted to 400 kPa total stress, constant suction path at 300 kPa and d) Sample compacted to 800 kPa total stress, constant suction path at 300 kPa,

ACCEPTED MANUSCRIPT

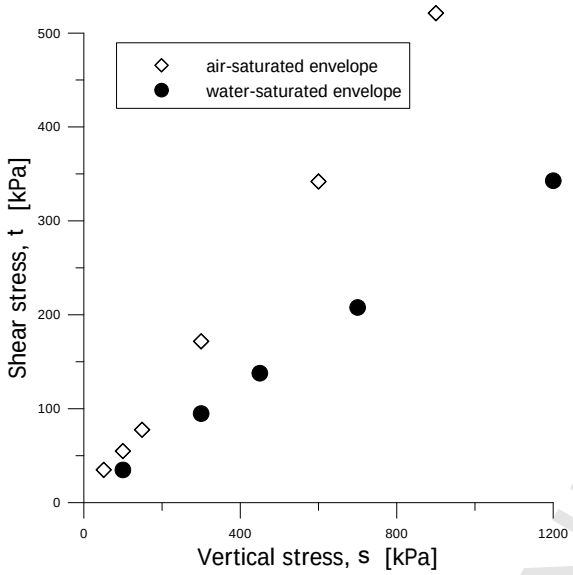

Figure 18. Water-saturated and air-saturated shear envelopes.

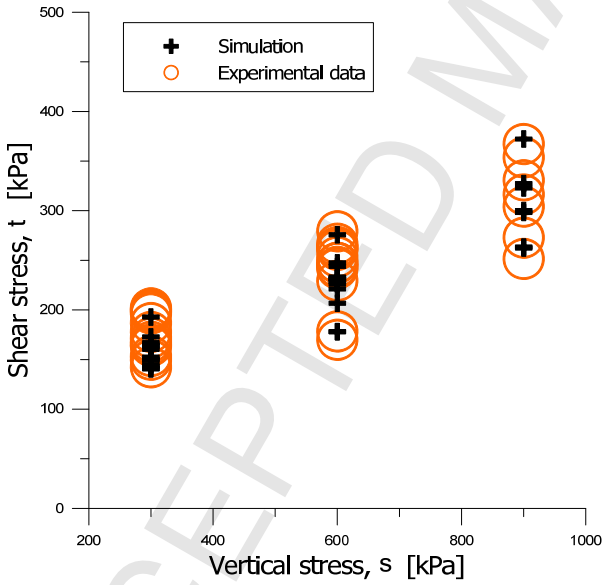

Figure 19. Ultimate shear simulation of kaolin compacted at different water contents and vertical stress.

ACCEPTED MANUSCRIPT

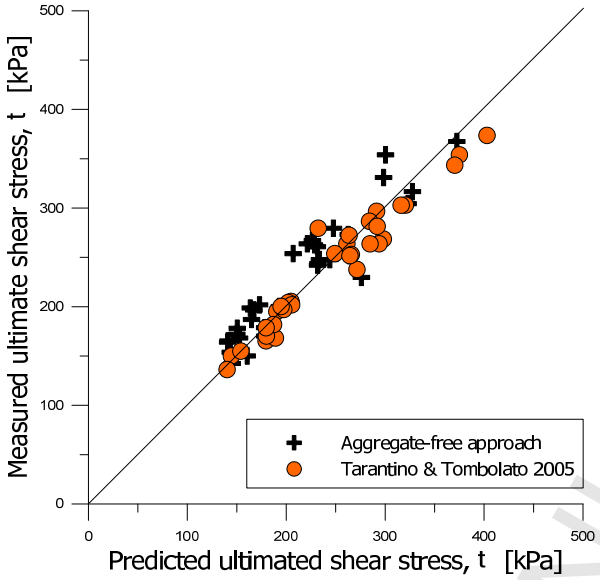

Figure 20 Prediction of the ultimate shear stress against the measured one.

ACCEPTED MANUSCRIPT

ACCEPTED MANUSCRIPT

Highlights

- A novel microstructure conceptual model is exploited to interpret a variety of mercury intrusion porosimetries from literature
- Two effective stresses for unsaturated states stemming from clay microstructure.
- Hydro-mechanical behaviour of compacted clay is modelled by only considering constitutive parameters from reconstituted clay and clay compressed by dry powder.
- Microstructure conceptual model to model volume change and shear strength behaviour of compacted clays.

ACCEPTED MANUSCRIPT